

**$M_4LiBe_4P_7O_{24}$ and $M_4Li(Li_3P)P_7O_{24}$ (M = Cs, Rb): deep-ultraviolet
nonlinear-optical phosphates with tetrahedra-substituted paracelsian-
like framework**

Yi-Gang Chen^a, Chunyu Yang^a, Fang Wang,^b Yao Guo*,^b Xingxing Jiang^c, Xian-
Ming Zhang*,^a

^aSchool of Chemistry & Material Science, Shanxi Normal University, Linfen, Shanxi 041004 China

^bSchool of Chemistry and Environment, Anyang Institute of Technology, Anyang 455000 China

^cBeijing Center for Crystal R&D, Technical Institute of Physics and Chemistry, Chinese Academy of Sciences, Beijing 100190, China

Contents

Section S1 Experimental Section, Characterization and Computational Method.

Table S1. Crystal data and structure refinement for $M_4LiBe_4P_7O_{24}$ and $MLiP_2O_6$ (M = Cs, Rb).

Table S2. Selected bond lengths (Å) and angles (deg) for (a) $M_4LiBe_4P_7O_{24}$ and (b) $MLiP_2O_6$ (M = Cs, Rb).

Table S3. Dipole moments of total polarization of one asymmetric unit in $M_4LiBe_4P_7O_{24}$ and $MLiP_2O_6$ (M = Cs, Rb).

Figure S1. X-ray powder diffraction patterns (a) $Cs_4LiBe_4P_7O_{24}$, (b) $Rb_4LiBe_4P_7O_{24}$, (c) $CsLiP_2O_6$, and (d) $RbLiP_2O_6$.

Figure S2. TG and DSC curves (a) $Cs_4LiBe_4P_7O_{24}$, (b) $Rb_4LiBe_4P_7O_{24}$, (c) $CsLiP_2O_6$, and (d) $RbLiP_2O_6$.

Figure S3. Photos of the crystals (a) $Cs_4LiBe_4P_7O_{24}$, (b) $Rb_4LiBe_4P_7O_{24}$, (c) $CsLiP_2O_6$, and (d) $RbLiP_2O_6$.

Figure S4. XPS spectra of $M_4LiBe_4P_7O_{24}$ (M = Cs, Rb).

Figure S5. XPS spectra of $MLiP_2O_6$ (M = Cs, Rb).

Figure S6. 1D zigzag chains of $[PO_3]_\infty$ in $MLiP_2O_6$ (M = Cs, Rb).

Figure S7. IR spectra (a) $M_4LiBe_4P_7O_{24}$ and (b) $MLiP_2O_6$ (M = Cs, Rb).

Figure S8. SHG signals for (a) $M_4LiBe_4P_7O_{24}$ and (b) $MLiP_2O_6$ (M = Cs, Rb) and KDP samples in the particle range 150–200 μm .

Figure S9. Electronic band structures (a) $Cs_4LiBe_4P_7O_{24}$, (b) $Rb_4LiBe_4P_7O_{24}$, (c) $CsLiP_2O_6$, and (d) $RbLiP_2O_6$.

References.

Section S1 Experimental Section, Characterization and Computational Method.

1. Experimental Section

1.1 Reagents

BeO (99.0%), Cs₂CO₃ (AR), Rb₂CO₃ (AR), LiF (99.0%), and NH₄H₂PO₄ (99.0%) were purchased from Aladdin and used as received.

1.2 Synthesis

M₄LiBe₄P₇O₂₄ (M = Rb, Cs)

Caution! Because of the high toxicity of beryllium oxide powder upon inhalation, all of the experiments were performed under sufficient ventilation.

Polycrystalline synthesis. The solid-state reaction is an important method for solid-material preparation, which has a wide application in lab and industry. The method offers the advantages including high yield, simple technology process, high selectivity, solvent-free, and so on. Polycrystalline samples of the titled compounds were obtained by solid-state reaction methods, which can provides a simple technology process to prepare the solid-materials on a large scale for further research and other potential researchers.

Pure polycrystalline samples of M₄LiBe₄P₇O₂₄ (M = Cs, Rb) were obtained using the stoichiometric amounts of the reactants (Cs₂CO₃ or Rb₂CO₃/LiF/BeO/NH₄H₂PO₄) by solid-state reaction methods. The raw materials Cs₂CO₃ (Rb₂CO₃), LiF, BeO, and NH₄H₂PO₄ in the molar ratio of 2: 1: 4: 7 were ground thoroughly in an agate mortar, pressed into a pellet, placed in a Pt crucible and preheated in a muffle furnace at 400 °C for 10 h to eliminate the water and gas. The mixtures were then heated to 760 °C for Cs₄LiBe₄P₇O₂₄ and 720 °C for Rb₄LiBe₄P₇O₂₄, and each then was sintered at that

temperature for 72 h with several intermediate grindings. Their phase purities were confirmed by powder X-ray diffraction (XRD) diffraction. About 45 mg of pure polycrystalline samples of $M_4LiBe_4P_7O_{24}$ ($M = Cs, Rb$) was separately calcined at 1050 °C for 0.5 h in a muffle furnace and their solidified melts were used to conduct the measurement of XRD patterns.

Crystal growth. Although analysis reveals that $M_4LiBe_4P_7O_{24}$ melt congruently, $M_4LiBe_4P_7O_{24}$ have high melting-temperatures 932 °C for $Cs_4LiBe_4P_7O_{24}$ and 1006 °C for $Rb_4LiBe_4P_7O_{24}$, respectively, which results in the obvious volatility of alkaline-metal cations Cs^+ and Rb^+ in the crystal-growth process of $M_4LiBe_4P_7O_{24}$. Therefore, crystal growths of $M_4LiBe_4P_7O_{24}$ ($M = Cs, Rb$) were fulfilled by using Cs_2O (Rb_2O)– LiF – P_2O_5 as the flux. For $Cs_4LiBe_4P_7O_{24}$, the raw materials Cs_2CO_3 , LiF , BeO and $NH_2H_2PO_4$ in the molar ratio of 1.5: 3: 1: 7 were ground thoroughly in an agate mortar, placed in a Pt crucible, preheated in a muffle furnace at 400 °C for 10 h to give off gas, next heated at 840 °C for 36 h to homogenize the solution, and finally slowly cooled to 600 °C at a rate of 3 °C/h before the furnace was turned off. Colorless crystals were then obtained after dissolving the flux in water.

For $Rb_4LiBe_4P_7O_{24}$, the raw materials Rb_2CO_3 , LiF , BeO and $NH_2H_2PO_4$ in the molar ratio of 1.5: 3: 1: 6 were ground thoroughly in an agate mortar, placed in a Pt crucible, preheated in a muffle furnace at 400 °C for 10 h to give off gas, next heated at 820 °C for 30 h to homogenize the solution, and finally slowly cooled to 600 °C at a rate of 3 °C/h before the furnace was turned off. Colorless block crystals were then obtained after dissolving the flux in water.

MLiP₂O₆ (M = Rb, Cs)

Polycrystalline synthesis. Pure polycrystalline samples of MLiP₂O₆ (M = Cs, Rb) were synthesized using the stoichiometric amounts of the reactants (Cs₂CO₃ or Rb₂CO₃/LiF/NH₄H₂PO₄). The raw materials Cs₂CO₃ (Rb₂CO₃), LiF, and NH₄H₂PO₄ in the molar ratio of 0.5: 1: 2 were ground thoroughly in an agate mortar, pressed into a pellet, placed in a Pt crucible and preheated in a muffle furnace at 300 °C for 10 h to eliminate the gas. The mixtures were then heated to 480 °C for MLiP₂O₆ (M = Cs, Rb) and each then was sintered at 480 °C for 48 h (42 h for RbLiP₂O₆) with several intermediate grindings until their powder XRD patterns kept unchanged. Their phase purities were confirmed by powder XRD diffraction. About 45 mg of pure polycrystalline samples of MLiP₂O₆ (M = Cs, Rb) was separately calcined at 700 °C for 0.5 h in a muffle furnace and their solidified melts were used to carry out the measurements of XRD patterns.

Crystal growth. Different from M₄LiBe₄P₇O₂₄, MLiP₂O₆ have relatively low melting-temperatures 665 or 681 °C, respectively, so their crystal growths of MLiP₂O₆ (M = Cs, Rb) were fulfilled by high-temperature melting method. Pure polycrystalline samples of MLiP₂O₆ (M = Cs, Rb) were separately heated at 700 °C for 2 h to homogenize the solutions, and slowly cooled to 350 °C at a rate of 2 °C/h (1.5 °C/h for RbLiP₂O₆). Colorless block crystals were achieved.

2. Property Characterization

2.1 Single crystal X-ray diffraction

Single crystal X-ray diffraction data were collected using an Agilent Technologies Gemini EOS diffractometer with EOS CCD detector at 293 K using Mo K α radiation

($\lambda = 0.71073 \text{ \AA}$). The collection of the intensity data, cell refinement, and data reduction were performed by the program *CrysAlisPro*. Colourless crystals were mounted on the tips of glass fibers for data collection. The structures were solved by direct methods with the program *SHELXS* and refined by the full-matrix least-squares program *SHELXL*.¹ Their structures had been carefully checked by *PLATON*² and no higher symmetries were recommended.

2.2 Powder X-ray diffraction (XRD)

XRD patterns of the polycrystalline samples were collected on a Rigaku MiniFlex II diffractometer using monochromated Cu K_{α} radiation ($\lambda = 1.540598 \text{ \AA}$) at room temperature in the 2θ range of 5° – 75° with a step size of 0.02° . The experimental powder X-ray diffraction patterns were found to be in good agreement with the calculated ones based on the single crystal crystallographic data (Figure S2).

2.3 Element analysis

Element analysis was performed by using a Jobin Yvon Ultima2 inductively coupled plasma optical emission spectrometer (ICP-OES) with Sepex Certiprep standards. The four crystal samples were dissolved in a concentrated hydrochloric acid. The inductively coupled plasma element analysis gave the molar ratios of 4.01: 1: 3.89: 7.06 for $\text{Cs}_4\text{LiBe}_4\text{P}_7\text{O}_{24}$, 3.99: 1: 3.98: 7.04 for $\text{Rb}_4\text{LiBe}_4\text{P}_7\text{O}_{24}$, 1.02: 1: 1.97 for CsLiP_2O_6 , and 1.05: 1: 2.09 for RbLiP_2O_6 , respectively, which are consistent with the molecular formula of the four compounds.

2.4 X-ray photoelectron spectroscopy (XPS).

The chemical states and surface compositions of the compound were investigated by a

Thermo scientific K-Alpha⁺ XPS with a monochromatic Al K α X-ray source (1486.6 eV) operating at 72 W (12 kV, 6 mA). All the XPS spectra underwent background subtraction and had been fitted using mixed Gaussian-Lorentzian peak shapes.

The XPS spectra of the compounds verify the existence of M, Li, Be, P, and O elements, respectively (Figure S4 and S5). For M₄LiBe₄P₇O₂₄ (M = Cs, Rb), the Cs3d and Rb3d XPS spectra (Figure S4b) show two main peaks at 737.78 and 723.78 eV for Cs3d_{3/2} and Cs3d_{5/2}, and 110.78 and 109.58 eV for Rb3d_{3/2} and Rb3d_{5/2}, which are assigned to the M3d_{3/2} and M3d_{5/2} binding energies for M⁺, respectively. The +1 oxidation state of Li is observed at 54.78 and 54.88 eV, respectively (Figure S4c). The peaks at 133.78 and 133.68 eV (Figure S4d) are P2p binding energies for the P (V) oxidation state. The O1s spectrum reveals the peaks at 531.18 eV (O²⁻) (Figure S4e). The Be1s XPS spectrum (Figure S4f) shows the peaks at 113.68 and 113.58 eV, respectively, which are attributed to the Be (II) oxidation state.

For MLiP₂O₆ (M = Cs, Rb), similarly, two main peaks at 737.98 and 724.08 eV for Cs3d_{3/2} and Cs3d_{5/2}, and 110.98 and 109.68 eV for Rb3d_{3/2} and Rb3d_{5/2} are assigned to the M3d_{3/2} and M3d_{5/2} binding energies for M⁺, respectively (Figure S5b). The +1 oxidation state of Li is found at 54.98 eV (Figure S5c). The peaks are observed at 134.08 and 133.68 eV, respectively, which is ascribed to P2p binding energies for the P (V) oxidation state (Figure S5d). The O1s XPS spectrum shows the peaks at 531.28 and 531.08 eV, respectively, which are the O (II) oxidation state (Figure S5e).

2.5 Thermal behavior

Thermal behavior analysis (Figure S3) was carried out on a simultaneous TGA/DSC

1 STARe System thermal analyzer instrument (DSC was calibrated by use of Al_2O_3). About 15 mg powders of the four compounds were placed in Pt crucibles, heated from room temperature to 1000 °C (1100 °C for $\text{Rb}_4\text{LiBe}_4\text{P}_7\text{O}_{24}$) at a rate of 10 °C/min under flowing N_2 atmosphere, respectively.

2.6 Infrared (IR) Spectroscopy Analysis

Fourier transform infrared (FTIR) spectra were recorded from KBr pellets in the range 2500–400 cm^{-1} on a Nicolet Model 5DX spectrometer. The IR spectra for $\text{M}_4\text{LiBe}_4\text{P}_7\text{O}_{24}$ and MLiP_2O_6 ($\text{M} = \text{Cs}, \text{Rb}$) are shown in Figure S4a and 4b.

$\text{Cs}_4\text{LiBe}_4\text{P}_7\text{O}_{24}$ and $\text{RbLiBe}_4\text{P}_7\text{O}_{24}$ have similar measurement patterns (Figure S4a). Peaks appear at 1310 and 1270 cm^{-1} , correspond to stretching vibrations of ν_{as} (O–P–O); peaks near 1160, 1115, and 1090 cm^{-1} are assigned to deformation vibrations (bridge vibrations) of ν_{s} (O–P–O); peaks between 960 and 923 cm^{-1} can be attributed to ν_{as} (P–O–P) and ν_{s} (P–O–P); peaks at 740 and 670 cm^{-1} are related to deformation vibrations of ν_{s} (O–P–O); peaks appear around 590 and 480 cm^{-1} are associated with fundamental frequency of PO_4 units; peaks between 1030 and 1000 cm^{-1} are assigned to the antisymmetric stretching vibrations of BeO_4 tetrahedra; peak near 780 cm^{-1} is designated to the bending mode of BeO_4 tetrahedra.

Also, CsLiP_2O_6 and RbLiP_2O_6 have similar frequency patterns (Figure S4b). Peaks at 1300 and 1270 cm^{-1} are correspond to stretching vibrations of ν_{as} (O–P–O); the 1160, 1105, and 1040 cm^{-1} peaks are attributed to deformation vibrations (bridge vibrations) of ν_{s} (O–P–O); peaks near 941 and 880 cm^{-1} is designated to ν_{as} (P–O–P) and ν_{s} (P–O–P); peaks at 757 and 682 cm^{-1} are related to deformation vibrations of ν_{s}

(O–P–O); peaks appear around 570 and 484 cm^{-1} are assigned to the fundamental frequency of PO_4 units.

2.7 UV-vis-NIR Diffuse Reflectance Spectroscopy

UV-vis-NIR diffuse reflection data for the four polycrystalline samples were recorded at room temperature using a powdered BaSO_4 sample as a standard (100% reflectance) on a PerkinElmer Lambda 950 UV/vis/NIR spectrophotometer. The scanning wavelength ranges from 190 nm to 1200 nm.

2.8 Second-Harmonic Generation

Powder second-harmonic generation (SHG) measurements were performed on the basis of the Kurtz-Perry method³ at 298 K. The measurements were carried out with a Q-switched Nd: YAG laser at a wavelength of 1064 nm. The four crystal samples were ground and sieved into a series of distinct size ranges: 25–40 μm , 40–63 μm , 63–80 μm , 80–125 μm , 125–150 μm , 150–200 μm , and 200–300 μm , respectively, which were pressed between glass slides and secured with tape in 1 mm thick aluminum holders containing a hole with diameter of 8 mm. Each of them was then placed into a light-tight box, and the intensity of the frequency-doubled output emitted from the samples was collected through a photomultiplier tube. Crystalline KH_2PO_4 (KDP) as the reference was ground and sieved into the same particle size ranges. The ratios of the SHG signals of the sample to the reference were calculated based on the intensity of second harmonic outputs in the same particle size range of 150–200 μm .

2.9 Computational method

Theoretical calculations were performed by using the Vienna Ab initio Simulation

Program (VASP 5.3).⁴ The structural and electronic properties were calculated by first principle calculations based on the density functional theory (DFT) employing the periodic plane-wave pseudopotential (PWPP) and the projector augmented wave (PAW) methods.⁵ The plane-wave cutoff energy was set as 600 eV. The reciprocal space integration was sampled using the Monkhorst-Pack scheme with a minimum spacing of 0.2 \AA^{-1} . The convergence criteria are set as 1.0^{-6} eV in total energy and 0.01 eV/\AA in atomic force, respectively. The geometrical optimizations were performed using the generalized gradient approximation of Perdew-Burke-Ernzerhof (GGA-PBE) method to describe the exchange-correlation energy.⁶ To improve the accuracy of GGA-PBE method, the hybrid functionals of the Heyd-Scuseria-Ernzerhof (HSE06) were further employed in the calculations of electronic DOS and band structures.⁷ The lengthgauge formalism⁸ was employed to predict the second-harmonic generation (SHG) coefficients at a zero frequency limit.

Table S1. Crystal data and structure refinement for $M_4LiBe_4P_7O_{24}$ and $MLiP_2O_6$ (M = Cs, Rb).

Empirical formula	$Cs_4LiBe_4P_7O_{24}$	$Rb_4LiBe_4P_7O_{24}$	$CsLiP_2O_6$	$RbLiP_2O_6$
Formula weight	1175.41	985.65	297.79	250.35
Temperature/K	293(2)	293(2)	293(2)	293(2)
Crystal system	orthorhombic	orthorhombic	orthorhombic	orthorhombic
Space group	$P222_1$	$P222_1$	$Fdd2$	$Fdd2$
$a/\text{\AA}$	13.0892(4)	12.8805(4)	19.0193(4)	19.0884(6)
$b/\text{\AA}$	13.0889(4)	12.9118(4)	19.3975(4)	18.5701(6)
$c/\text{\AA}$	13.2528(4)	12.9447(4)	13.1986(3)	13.0448(4)
$\alpha/^\circ$	90	90	90	90
$\beta/^\circ$	90	90	90	90
$\gamma/^\circ$	90	90	90	90
Volume/ \AA^3	2270.51(12)	2152.84(12)	4869.32(18)	4624.1(2)
Z	4	4	32	32
$\rho_{\text{calc}} \text{ g/cm}^3$	3.439	3.041	3.250	2.877
μ/mm^{-1}	6.974	9.674	6.570	9.078
$F(000)$	2144.0	1856.0	4352.0	3776.0
GOF on F^2	0.933	1.050	1.161	1.070
$R_1, wR_2 [I \geq 2\sigma(I)]$	0.0270, 0.0520	0.0266, 0.0499	0.0324, 0.0769	0.0352, 0.0829
$R_1, wR_2 [\text{all data}]$	0.0314, 0.0542	0.0362, 0.0524	0.0330, 0.0772	0.0389, 0.0851
Largest diff. peak/hole / $e \text{ \AA}^{-3}$	0.99/−0.50	0.62/−0.50	1.86/−1.22	0.74/−0.60
Flack parameter	−0.030(10)	−0.007(4)	0.007(8)	−0.001(7)

$$^a R_1 = \sum ||F_o| - |F_c|| / \sum |F_o|. \quad wR_2 = [\sum w(F_o^2 - F_c^2)^2 / \sum w(F_o^2)^2]^{1/2}.$$

Table S2. Selected bond lengths (Å) and angles (deg) for (a) $M_4LiBe_4P_7O_{24}$ and (b) $MLiP_2O_6$ (M = Cs, Rb).

(a)					
$Cs_4LiBe_4P_7O_{24}$					
P1–O2	1.603(3)	Li1–O4 ^{#17}	1.869(7)	O8–P1–O1	115.07(17)
P1–O8	1.500(3)	Li1–O3 ^{#2}	1.920(8)	O8–P1–O7	111.67(18)
P1–O1	1.503(3)	Li1–O18 ^{#8}	1.994(8)	O1–P1–O7	113.33(18)
P1–O7	1.510(3)	Li1–O15	1.876(7)	O8–P1–O2	106.27(19)
P2–O2	1.594(3)	Cs1–O15 ^{#1}	3.071(3)	O1–P1–O2	101.29(16)
P2–O3	1.470(3)	Cs1–O5	3.071(3)	O7–P1–O2	108.20(17)
P2–O4	1.462(3)	Cs1–O14	3.103(3)	O4–P2–O3	121.2(2)
P2–O5	1.590(3)	Cs1–O4 ^{#2}	3.331(4)	O4–P2–O2	108.8(2)
P3–O5	1.609(3)	Cs1–O4	3.338(4)	O3–P2–O2	105.82(18)
P3–O6	1.503(3)	Cs1–O7	3.353(3)	O4–P2–O5	103.43(18)
P3–O9	1.495(3)	Cs1–O13	3.427(3)	O3–P2–O5	111.59(19)
P3–O10	1.504(3)	Cs1–O15	3.483(4)	O2–P2–O5	104.97(16)
P4–O12	1.504(3)	Cs1–O12	3.526(3)	O9–P3–O6	113.82(17)
P4–O14	1.601(3)	Cs1–O9	3.590(3)	O9–P3–O10	115.17(18)
P4–O20	1.499(3)	Cs1–O5 ^{#2}	3.615(3)	O6–P3–O10	110.51(17)
P4–O21	1.487(3)	Cs1–O14 ^{#1}	3.686(4)	O9–P3–O5	102.30(18)
P5–O14	1.607(4)	Cs2–O24 ^{#6}	3.090(3)	O6–P3–O5	107.14(17)
P5–O16	1.573(4)	Cs2–O11	3.209(3)	O10–P3–O5	107.02(17)
P5–O18	1.465(4)	Cs2–O8	3.243(3)	O21–P4–O20	108.85(18)
P5–O15	1.470(3)	Cs2–O8 ^{#3}	3.302(3)	O21–P4–O12	116.06(19)
P6–O16	1.620(4)	Cs2–O24	3.324(3)	O20–P4–O12	113.49(19)
P6–O17	1.503(3)	Cs2–O7	3.338(3)	O21–P4–O14	107.9(2)
P6–O19	1.485(3)	Cs2–O12	3.344(3)	O20–P4–O14	108.74(17)
P7–O23	1.516(4)	Cs2–O9	3.395(3)	O12–P4–O14	101.25(18)
P7–O11	1.510(3)	Cs2–O11 ^{#3}	3.412(3)	O18–P5–O15	120.8(2)
P7–O22	1.511(4)	Cs2–O19 ^{#6}	3.449(3)	O18–P5–O16	109.56(19)
P7–O24	1.536(3)	Cs2–O19	3.545(3)	O15–P5–O16	106.31(17)
Be1–O1 ^{#3}	1.628(6)	Cs3–O18 ^{#6}	3.085(3)	O18–P5–O14	110.87(18)
Be1–O21 ^{#1}	1.613(6)	Cs3–O6 ^{#5}	3.150(3)	O19–P6–O17	114.80(18)
Be1–O12	1.607(7)	Cs3–O3 ^{#5}	3.155(4)	O19–P6–O13	112.08(18)
Be1–O7	1.640(7)	Cs3–O17 ^{#14}	3.195(3)	O17–P6–O13	113.14(19)
Be2–O6 ^{#3}	1.654(5)	Cs3–O23 ^{#15}	3.206(3)	O19–P6–O16	108.91(19)
Be2–O8 ^{#3}	1.659(7)	Cs3–O22 ^{#15}	3.324(3)	O22–P7–O23	105.33(16)
Be2–O12	1.593(6)	Cs3–O16 ^{#14}	3.495(3)	O11 ^{#6} –P7–O24	107.37(16)

Be2-O23	1.594(6)	Cs4-O18 ^{#16}	3.086(3)	O22-P7-O24	112.01(17)
Be3-O17 ^{#14}	1.616(6)	Cs4-O1 ^{#11}	3.306(3)	O23-P7-O24	109.87(18)
Be3-O9 ^{#2}	1.627(7)	Cs4-O23 ^{#3}	3.357(3)	O12-Be1-O21 ^{#1}	112.0(4)
Be3-O13 ^{#2}	1.644(7)	Cs4-O21 ^{#3}	3.426(3)	O21 ^{#1} -Be1-O1 ^{#3}	109.2(3)
Be3-O10	1.633(6)	Cs4-O2 ^{#11}	3.605(3)	O12-Be1-O7	105.3(3)
Be4-O22 ^{#12}	1.603(6)	Cs3-O17 ^{#14}	3.195(3)	O1 ^{#3} -Be1-O7	111.3(4)
Be4-O20	1.652(6)	Cs3-O23 ^{#15}	3.206(3)	O23-Be2-O11	114.9(4)
Be4-O19	1.676(6)	Cs3-O22 ^{#15}	3.324(3)	O23-Be2-O6 ^{#3}	105.8(3)
Be4-O24	1.575(6)	Cs3-O16 ^{#14}	3.495(3)	O11-Be2-O6 ^{#3}	110.7(4)
Cs3-O10 ^{#5}	3.520(3)	Cs4-O20 ^{#3}	3.343(3)	O23-Be2-O8 ^{#3}	111.5(4)
Cs3-O17 ^{#6}	3.566(3)	Cs4-O3	3.413(3)	O17 ^{#14} -Be3-O9 ^{#2}	109.3(4)
Cs4-O22 ^{#3}	3.090(3)	Cs4-O21 ^{#16}	3.494(3)	O17 ^{#14} -Be3-O10	111.1(3)
Cs4-O20 ^{#16}	3.175(3)	Cs4-O20 ^{#3}	3.343(3)	O9 ^{#2} -Be3-O10	111.7(4)
O24-Be4-O22 ^{#12}		114.9(3)		O17 ^{#14} -Be3-O13 ^{#2}	110.7(4)
O24-Be4-O20		111.4(4)		O24-Be4-O19	106.7(4)
O4 ^{#17} -Li1-O15		103.1(3)		O22 ^{#12} -Be4-O20	103.6(3)
O4 ^{#17} -Li1-O3 ^{#2}		118.3(4)		O15-Li1-O3 ^{#2}	109.8(4)
Rb ₄ LiBe ₄ P ₇ O ₂₄					
P1-O23	1.500(2)	Li1-O17 ^{#5}	1.876(6)	O23-P1-O9	114.69(13)
P1-O13	1.504(2)	Li1-O16 ^{#15}	1.901(5)	O23-P1-O13	113.80(14)
P1-O14	1.615(2)	Li1-O5 ^{#9}	1.979(6)	O23-P1-O14	102.06(12)
P1-O9	1.502(2)	Li1-O6	1.891(6)	O9-P1-O14	106.57(13)
P2-O14	1.598(2)	Rb1-O20	2.838(2)	O13-P1-O14	106.43(12)
P2-O16	1.468(2)	Rb1-O1 ^{#6}	2.998(2)	O16-P2-O17	121.77(15)
P2-O17	1.474(2)	Rb1-O14 ^{#2}	3.039(2)	O16-P2-O14	109.16(14)
P2-O24	1.614(2)	Rb1-O5 ^{#1}	3.239(3)	O17-P2-O14	105.53(13)
P3-O15	1.503(2)	Rb1-O21	3.270(2)	O16-P2-O24	104.38(13)
P3-O18	1.506(2)	Rb1-O2 ^{#6}	3.313(2)	O14-P2-O24	104.98(12)
P3-O22	1.506(2)	Rb1-O4 ^{#1}	3.329(3)	O15-P3-O18	113.88(13)
P3-O24	1.619(2)	Rb1-O1 ^{#1}	3.473(2)	O15-P3-O22	113.00(12)
P4-O1	1.5107(19)	Rb1-O2 ^{#1}	3.489(3)	O18-P3-O22	110.70(12)
P4-O2	1.484(2)	Rb1-O23 ^{#2}	3.491(2)	O15-P3-O24	104.14(12)
P4-O3	1.504(2)	Rb1-O17 ^{#2}	3.530(3)	O22-P3-O24	106.94(12)
P4-O4	1.588(2)	Rb1-O14 ^{#7}	3.631(2)	O2-P4-O3	113.32(15)
P5-O4	1.581(2)	Rb2-O5 ^{#1}	2.772(2)	O2-P4-O1	109.68(13)
P5-O5	1.474(2)	Rb2-O22 ^{#2}	2.8549(19)	O3-P4-O1	114.82(13)
P5-O6	1.471(2)	Rb2-O10 ^{#3}	3.0344(19)	O2-P4-O4	108.66(15)
P5-O7	1.593(2)	Rb2-O15	3.253(2)	O1-P4-O4	104.16(12)
P6-O7	1.613(2)	Rb2-O22	3.258(2)	O6-P5-O5	120.51(15)
P6-O8	1.494(2)	Rb2-O20	3.262(2)	O6-P5-O4	105.06(14)
P6-O10	1.518(2)	Rb2-O19	3.312(2)	O5-P5-O4	107.70(16)
P7-O19	1.515(2)	Rb2-O17 ^{#2}	3.361(3)	O6-P5-O7	105.81(13)

P7-O20	1.530(2)	Rb2-O10 ^{#1}	3.368(2)	O4-P5-O7	105.53(13)
P7-O21	1.527(2)	Rb2-O21	3.401(2)	O8-P6-O11	112.84(13)
P7-O12 ^{#10}	1.532(2)	Rb3-O12	2.8389(19)	O8-P6-O10	112.74(12)
Be1-O9 ^{#4}	1.618(5)	Rb3-O13	2.961(2)	O11-P6-O10	113.58(12)
Be1-O23 ^{#16}	1.621(4)	Rb3-O11	2.964(2)	O8-P6-O7	108.15(12)
Be1-O3 ^{#4}	1.639(5)	Rb3-O12 ^{#1}	3.246(2)	O10-P6-O7	106.69(12)
Be1-O1	1.617(4)	Rb3-O13 ^{#10}	3.292(2)	O19-P7-O21	112.13(13)
Be2-O19 ^{#2}	1.561(5)	Rb3-O21 ^{#8}	3.417(2)	O19-P7-O20	108.88(13)
Be2-O22 ^{#2}	1.655(4)	Rb3-O3	3.430(2)	O21-P7-O20	106.14(12)
Be2-O13 ^{#2}	1.683(4)	Rb3-O19 ^{#10}	3.470(2)	O19-P7-O12 ^{#10}	108.29(12)
Be2-O21	1.589(4)	Rb3-O8 ^{#1}	3.476(2)	O20-P7-O12 ^{#10}	111.81(13)
Be3-O18 ^{#5}	1.626(4)	Rb3-O8	3.486(2)	O1-Be1-O9 ^{#4}	112.2(3)
Be3-O10 ^{#1}	1.665(4)	Rb3-O23 ^{#10}	3.534(3)	O1-Be1-O23 ^{#16}	107.3(3)
Be3-O11	1.634(4)	Rb4-O6 ^{#4}	2.844(2)	O9 ^{#4} -Be1-O23 ^{#16}	112.2(3)
Be3-O15	1.600(4)	Rb4-O24	2.942(2)	O1-Be1-O3 ^{#4}	110.3(3)
Be4-O8 ^{#1}	1.631(4)	Rb4-O3	3.027(2)	O19 ^{#2} -Be2-O21	118.1(3)
Be4-O2 ^{#1}	1.633(4)	Rb4-O7	3.067(2)	O19 ^{#2} -Be2-O22 ^{#2}	108.6(3)
Be4-O20	1.603(4)	Rb4-O16	3.171(3)	O21-Be2-O22 ^{#2}	107.5(3)
Be4-O12	1.600(4)	Rb4-O6	3.236(3)	O19 ^{#2} -Be2-O13 ^{#2}	105.4(3)
Rb4-O4 ^{#4}	3.549(3)	Rb4-O9	3.394(2)	O15-Be3-O18 ^{#5}	111.6(2)
Rb4-O18 ^{#5}	3.571(2)	Rb4-O11	3.487(2)	O15-Be3-O11	106.2(2)
Rb4-O16 ^{#5}	3.546(3)	Rb4-O17 ^{#5}	3.503(3)	O18 ^{#5} -Be3-O11	108.7(2)
O17 ^{#5} -Li1-O6		106.8(3)		O18 ^{#5} -Be3-O10 ^{#1}	112.1(2)
O17 ^{#5} -Li1-O16 ^{#15}		117.6(3)		O12-Be4-O20	114.8(3)
O6-Li1-O16 ^{#15}		107.7(3)		O12-Be4-O8 ^{#1}	106.5(2)
O17 ^{#5} -Li1-O5 ^{#9}		101.1(3)		O20-Be4-O8 ^{#1}	110.6(3)
O6-Li1-O5 ^{#9}		116.6(3)		O20-Be4-O2 ^{#1}	107.5(2)

Symmetry transformations used to generate equivalent atoms:

$\text{Cs}_4\text{LiBe}_4\text{P}_7\text{O}_{24}$:

#1 $x, -y, -z$; #2 $-x, y, -z+1/2$; #3 $-x-1, y, -z+1/2$; #5 $x, -y-1, -z+1$; #6 $x, -y-1, -z$;

#8 $-x, y, -z-1/2$; #11 $x, -y, -z+1$; #12 $-x-1, y, -z-1/2$; #14 $-x, -y-1, z+1/2$;

#15 $-x-1, -y-1, z+1/2$; #16 $x, y, z+1$; #17 $-x, -y, z-1/2$.

$\text{Rb}_4\text{LiBe}_4\text{P}_7\text{O}_{24}$:

#1 $-x+1, y, -z-1/2$; #2 $-x+1, y, -z+1/2$; #3 $-x+1, -y, z+1/2$; #4 $-x, y, -z-1/2$; #5 $x, -y, -z$;

#6 $-x+1, -y+1, z+1/2$; #7 $x+1, y, z$; #8 $-x+1, -y+1, z-1/2$; #9 $x, -y, -z-1$; #10 $x, -y+1, -z$;

#15 $-x, -y, z-1/2$; #16 $-x, -y+1, z-1/2$.

(b)

CsLiP ₂ O ₆					
P1-O1	1.469(4)	Cs1-O1 ^{#5}	3.355(5)	O1-P1-O3	120.7(3)
P1-O2	1.596(4)	Cs1-O2 ^{#4}	3.280(4)	O1-P1-O2	111.0(3)
P1-O3	1.469(5)	Cs1-O2 ^{#6}	3.562(5)	O2-P1-O3	103.8(3)
P1-O10 ^{#3}	1.606(4)	Cs1-O3 ^{#4}	3.555(6)	O1-P1-O10 ^{#3}	108.3(3)
P2-O9	1.599(4)	Cs1-O3 ^{#6}	3.452(6)	O3-P1-O10 ^{#3}	111.3(3)
P2-O10	1.619(4)	Cs1-O4 ^{#7}	3.643(6)	O2-P1-O10 ^{#3}	99.6(2)
P2-O11	1.483(5)	Cs1-O5 ^{#8}	3.730(5)	O10-P2-O9	102.6(2)
P2-O12	1.475(4)	Cs1-O6 ^{#2}	3.400(5)	O10-P2-O11	107.2(3)
P3-O6	1.479(4)	Cs1-O8 ^{#2}	3.127(4)	O10-P2-O12	108.0(3)
P3-O7	1.490(4)	Cs1-O10	3.331(5)	O9-P2-O11	106.9(3)
P3-O8	1.610(4)	Cs1-O11 ^{#3}	3.103(4)	O9-P2-O12	112.2(2)
P3-O9	1.602(5)	Cs1-O12	3.452(5)	O11-P2-O12	118.7(3)
P4-O2 ^{#10}	1.594(4)	Cs2-O1	3.100(4)	O8-P3-O6	105.2(2)
P4-O4	1.486(5)	Cs2-O4	3.529(6)	O8-P3-O7	111.0(2)
P4-O5	1.483(4)	Cs2-O5	3.740(5)	O8-P3-O9	97.3(2)
P4-O8 ^{#3}	1.599(4)	Cs2-O5 ^{#2}	3.225(5)	O7-P3-O9	110.5(3)
Li1-O3 ^{#6}	1.900(11)	Cs2-O6 ^{#2}	3.318(5)	O6-P3-O9	110.6(3)
Li1-O6	1.860(11)	Cs2-O7 ^{#1}	2.992(4)	O6-P3-O7	119.9(3)
Li1-O11 ^{#3}	1.972(13)	Cs2-O8 ^{#3}	3.690(4)	O5-P4-O4	119.5(3)
Li1-O12 ^{#9}	2.006(12)	Cs2-O9 ^{#3}	3.295(4)	O5-P4-O2 ^{#10}	106.5(3)
Li2-O1 ^{#15}	1.969(11)	Cs2-O11 ^{#3}	3.385(5)	O5-P4-O8 ^{#3}	111.7(2)
Li2-O4	1.904(12)	Cs2-O12	2.963(4)	O4-P4-O2 ^{#10}	109.3(3)
Li2-O5 ^{#1}	1.941(12)	Cs2-O7	3.491(4)	O4-P4-O8 ^{#3}	105.4(3)
Li2-O7 ^{#1}	1.942(11)	Cs2-O9	3.395(3)	O2 ^{#10} -P4-O8 ^{#3}	103.3(2)
O3 ^{#6} -Li1-O12 ^{#9}		110.4(5)		O6-Li1-O3 ^{#6}	105.1(5)
O11 ^{#3} -Li1-O12 ^{#9}		121.8(5)		O6-Li1-O11 ^{#3}	111.7(5)
O4-Li2-O7 ^{#1}		112.3(6)		O6-Li1-O12 ^{#9}	100.1(6)
O4-Li2-O5 ^{#1}		119.7(6)		O3 ^{#6} -Li1-O11 ^{#3}	106.6(6)
O4-Li2-O1 ^{#15}		102.9(5)		O7 ^{#1} -Li2-O1 ^{#15}	110.0(6)
O7 ^{#1} -Li2-O5 ^{#1}		110.4(5)		O5 ^{#1} -Li2-O1 ^{#15}	100.3(5)
RbLiP ₂ O ₆					
P1-O7	1.475(3)	Rb1-O1 ^{#3}	3.101(4)	O7-P1-O10	109.07(19)
P1-O10	1.601(3)	Rb1-O3	3.478(4)	O7-P1-O11	110.3(2)
P1-O11	1.587(4)	Rb1-O3 ^{#2}	2.874(4)	O7-P1-O12	121.2(3)
P1-O12	1.465(4)	Rb1-O5 ^{#3}	3.230(4)	O10-P1-O11	100.3(2)
P2-O6	1.485(4)	Rb1-O6	3.247(4)	O10-P1-O12	110.3(2)
P2-O8	1.594(3)	Rb1-O7	2.982(3)	O11-P1-O12	103.5(2)

P2–O9	1.483(3)	Rb1–O8	3.217(3)	O6–P2–O8	105.87(19)
P2–O10	1.616(3)	Rb1–O9 ^{#1}	2.828(3)	O6–P2–O9	119.6(2)
P3–O3	1.480(4)	Rb2–O2 ^{#7}	3.484(5)	O6–P2–O10	108.4(2)
P3–O4	1.612(3)	Rb2–O4 ^{#3}	2.975(3)	O8–P2–O9	111.45(19)
P3–O5	1.475(4)	Rb2–O5 ^{#3}	3.358(4)	O8–P2–O10	103.46(19)
P3–O8 ^{#1}	1.611(3)	Rb2–O6	2.920(3)	O9–P2–O10	106.8(2)
P4–O1	1.475(4)	Rb2–O7 ^{#6}	3.289(4)	O3–P3–O4	111.08(19)
P4–O2	1.479(4)	Rb2–O9 ^{#1}	3.503(4)	O3–P3–O5	120.2(2)
P4–O4 ^{#9}	1.604(3)	Rb2–O10 ^{#1}	3.058(3)	O3–P3–O8 ^{#1}	110.2(2)
P4–O11 ^{#10}	1.603(4)	Rb2–O11 ^{#1}	3.570(4)	O4–P3–O5	105.2(2)
Li1–O5 ^{#12}	1.866(9)	Rb2–O11 ^{#5}	3.170(3)	O4–P3–O8 ^{#1}	96.95(17)
Li1–O6 ^{#12}	2.001(9)	Rb2–O12 ^{#1}	3.564(5)	O5–P3–O8 ^{#1}	110.7(2)
Li1–O9	1.969(8)	Rb2–O12 ^{#5}	3.396(4)	O1–P4–O2	120.6(2)
Li1–O12 ^{#5}	1.903(8)	Rb2–O12 ^{#6}	3.535(5)	O1–P4–O4 ^{#9}	110.8(2)
Li2–O1 ^{#2}	1.904(9)	Li2–O3 ^{#2}	1.950(9)	O1–P4–O11 ^{#10}	106.6(2)
Li2–O2	1.894(10)	Li2–O7 ^{#14}	1.947(9)	O2–P4–O4 ^{#9}	105.5(2)
O9–Li1–O12 ^{#5}		105.8(4)		O2–P4–O11 ^{#10}	108.9(3)
O1 ^{#2} –Li2–O2		120.7(5)		O4 ^{#9} –P4–O11 ^{#10}	103.23(19)
O1 ^{#2} –Li2–O3 ^{#2}		109.9(4)		O5 ^{#12} –Li1–O6 ^{#12}	110.2(4)
O1 ^{#2} –Li2–O7 ^{#14}		100.9(4)		O5 ^{#12} –Li1–O9	100.1(4)
O2–Li2–O3 ^{#2}		112.0(5)		O5 ^{#12} –Li1–O12 ^{#5}	105.1(4)
O2–Li2–O7 ^{#14}		101.1(4)		O6 ^{#12} –Li1–O9	123.6(4)
O3 ^{#2} –Li2–O7 ^{#14}		110.9(4)		O6 ^{#12} –Li1–O12 ^{#5}	110.2(5)

Symmetry transformations used to generate equivalent atoms:

CsLiP₂O₆:

#1 $-x-1/2, -y-3/2, z$; #2 $x+1/4, -y-5/4, z-1/4$; #3 $-x-3/4, y+1/4, z+1/4$;
 #4 $x-1/4, -y-3/4, z-1/4$; #5 $-x-1/2, -y-1, z-1/2$; #6 $-x-3/4, y-1/4, z-1/4$;
 #7 $x-1/4, -y-5/4, z-3/4$; #8 $-x-3/4, y+1/4, z-3/4$; #9 $x-1/4, -y-5/4, z+1/4$;
 #10 $-x-1/2, -y-1, z+1/2$; #15 $-x-1/4, y-1/4, z+1/4$.

RbLiP₂O₆:

#1 $x-1/4, -y+1/4, z-1/4$; #2 $-x+1/2, -y+1/2, z$; #3 $-x+3/4, y+1/4, z-1/4$;
 #5 $-x+5/4, y-1/4, z-1/4$; #6 $-x+1, -y+1/2, z-1/2$; #7 $-x+3/4, y-1/4, z-3/4$;
 #9 $x+1/4, -y+1/4, z+1/4$; #10 $-x+1, -y+1/2, z+1/2$; #12 $-x+1, -y, z$;
 #14 $x-1/4, -y+3/4, z+1/4$.

Table S3. Dipole moments of total polarization of one asymmetric unit in $M_4LiBe_4P_7O_{24}$ and $MLiP_2O_6$ ($M = Cs, Rb$).

(a) $Cs_4LiBe_4P_7O_{24}$

Polar units	Dipole moment (Debye)			
	x/a	y/b	z/c	Total magnitude
$\sum_{k=1}^4 (BeO_4)_k$	1.95	1.45	1.47	2.84
$\sum_{k=1}^7 (PO_4)_k$	3.59	4.40	2.67	6.27
$\sum_{k=1}^1 (LiO_4)_k$	0.51	-0.69	-0.18	0.88
$\sum_{k=1}^4 (CsO_n)_k$	-1.97	-0.23	5.78	6.11
Asymmetric unit	4.08	4.93	9.74	11.65
Unit cell ($Z = 4$)	0.00	0.00	0.00	0.00

(b) $Rb_4LiBe_4P_7O_{24}$

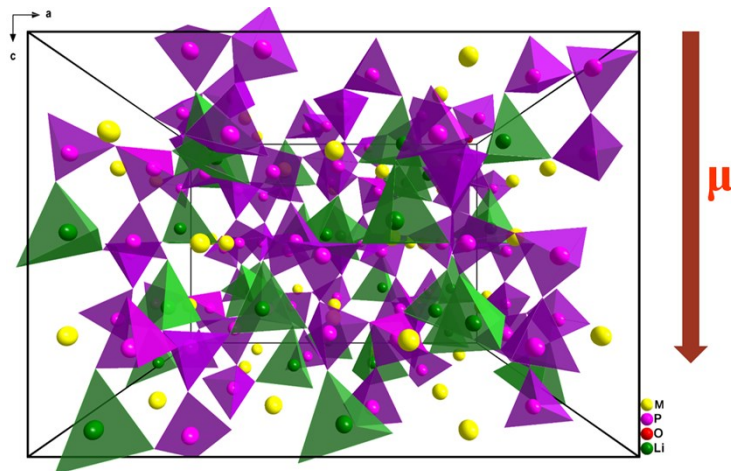
Polar units	Dipole moment (Debye)			
	x/a	y/b	z/c	Total magnitude
$\sum_{k=1}^4 (BeO_4)_k$	1.50	-0.38	0.82	1.75
$\sum_{k=1}^7 (PO_4)_k$	-4.79	-0.71	1.69	5.13
$\sum_{k=1}^1 (LiO_4)_k$	0.85	-0.40	-0.11	0.95
$\sum_{k=1}^4 (RbO_n)_k$	-9.12	5.75	-5.86	12.27
Asymmetric unit	-11.56	4.26	-3.46	12.80
Unit cell ($Z = 4$)	0.00	0.00	0.00	0.00

(c) CsLiP₂O₆

Polar units	Dipole moment (Debye)			
	x/a	y/b	z/c	Total magnitude
$\sum_{K=1}^4 (PO_4)_K$	-9.24	1.90	-4.36	10.40
$\sum_{K=1}^2 (LiO_4)_K$	-2.61	-1.86	0.22	3.21
$\sum_{k=1}^2 (CsOn)_k$	4.79	-9.37	-1.74	10.67
Asymmetric unit	-7.06	-9.33	-5.88	13.09
Unit cell ($Z = 32$)	0.00	0.00	-109.91	109.91

(d) RbLiP₂O₆

Polar units	Dipole moment (Debye)			
	x/a	y/b	z/c	Total magnitude
$\sum_{K=1}^4 (PO_4)_K$	6.24	0.52	-4.47	7.69
$\sum_{K=1}^2 (LiO_4)_K$	-0.64	2.18	-0.56	2.34
$\sum_{k=1}^2 (RbOn)_k$	7.13	-1.31	-3.80	8.19
Asymmetric unit	12.73	1.39	-8.83	15.55
Unit cell ($Z = 32$)	0.00	0.00	-144.26	144.26

**(e) MLiP₂O₆ with the net polarization along the c -axis direction (μ , dipole moment; arrow represents direction)**

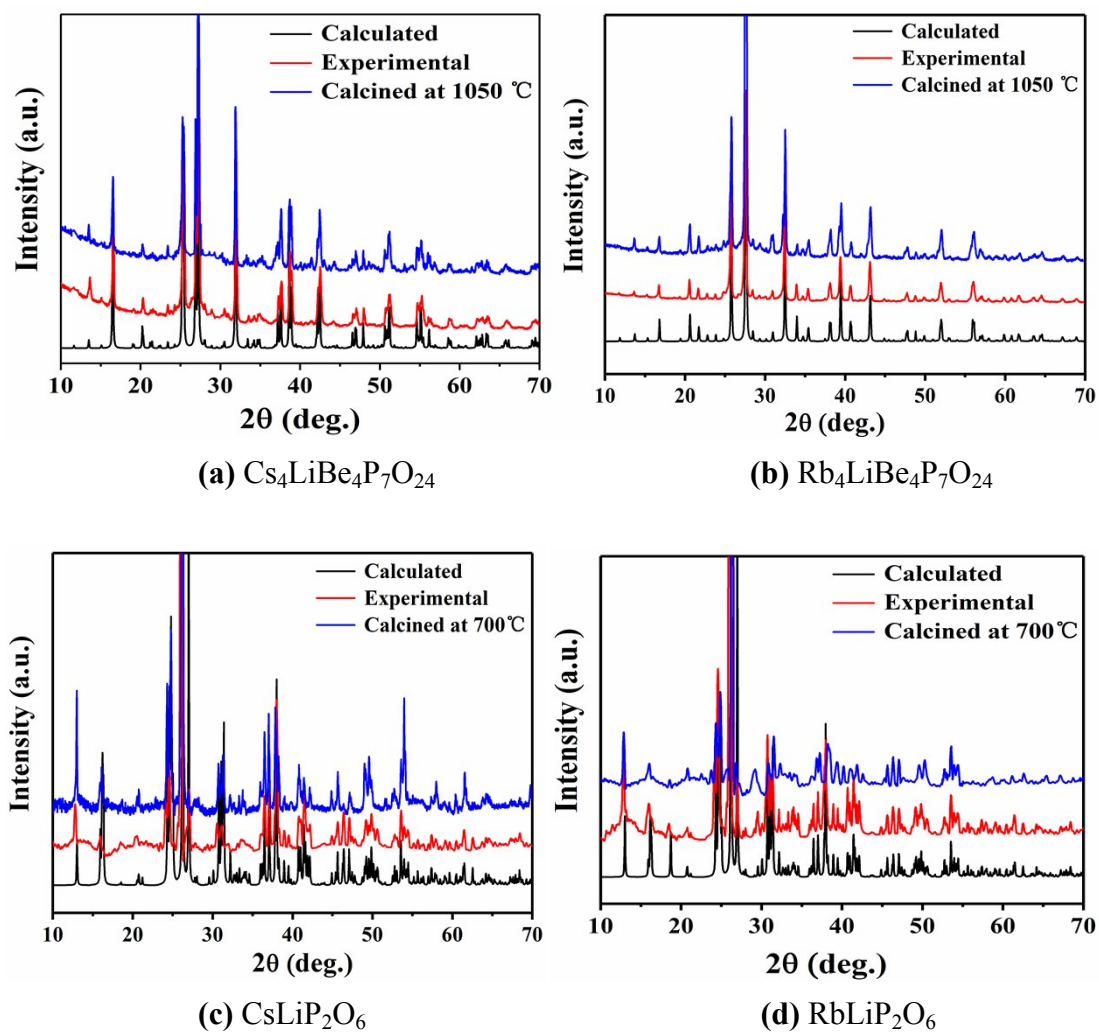


Figure S1. X-ray powder diffraction patterns (a) $\text{Cs}_4\text{LiBe}_4\text{P}_7\text{O}_{24}$, (b) $\text{Rb}_4\text{LiBe}_4\text{P}_7\text{O}_{24}$, (c) CsLiP_2O_6 , and (d) RbLiP_2O_6 .

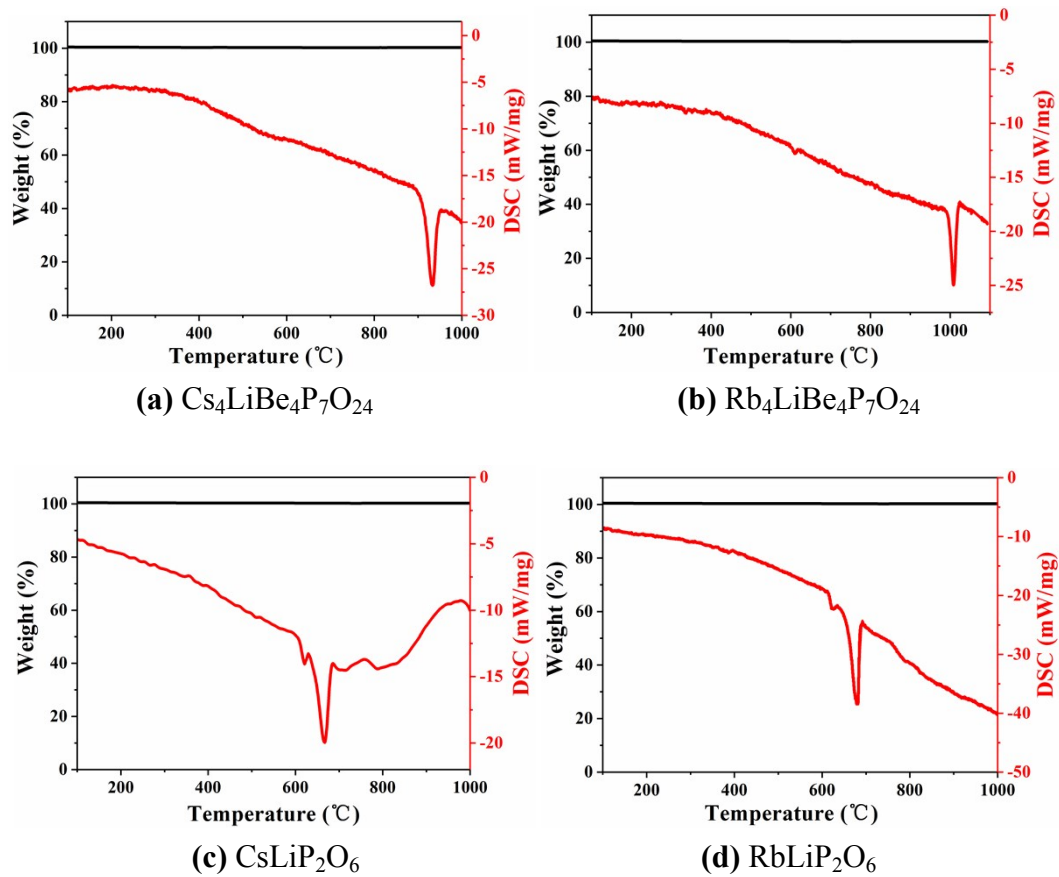
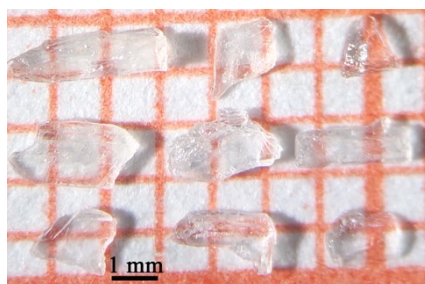
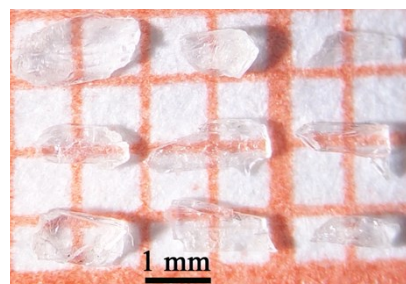


Figure S2. TG and DSC curves (a) $\text{Cs}_4\text{LiBe}_4\text{P}_7\text{O}_{24}$, (b) $\text{Rb}_4\text{LiBe}_4\text{P}_7\text{O}_{24}$, (c) CsLiP_2O_6 , and (d) RbLiP_2O_6 .



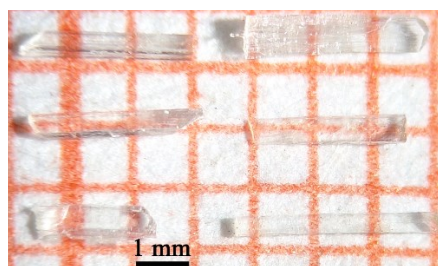
(a) Cs₄LiBe₄P₇O₂₄



(b) Rb₄LiBe₄P₇O₂₄



(c) CsLiP₂O₆



(d) RbLiP₂O₆

Figure S3. Photos of the crystals (a) Cs₄LiBe₄P₇O₂₄, (b) Rb₄LiBe₄P₇O₂₄, (c) CsLiP₂O₆, and (d) RbLiP₂O₆.

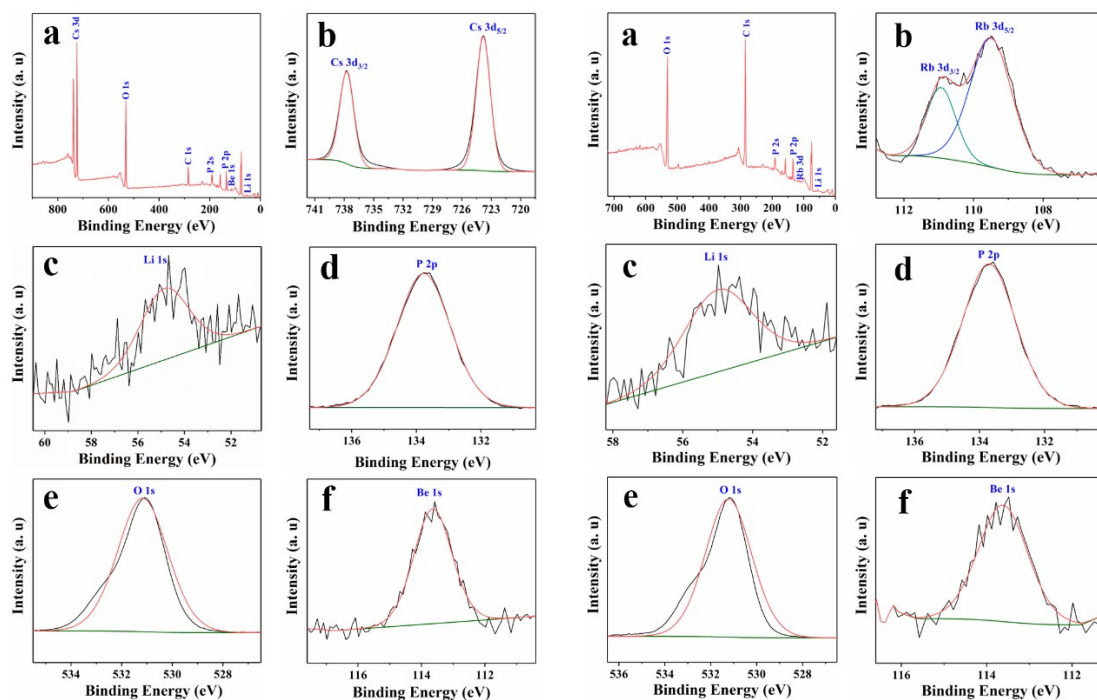


Figure S4 (a) XPS spectra of $M_4LiBe_4P_7O_{24}$. (b) M3d, (c) Li1s, (d) P2p ($2p_{3/2}$), (e) O1s, and (f) Be1s high-resolution XPS spectra.

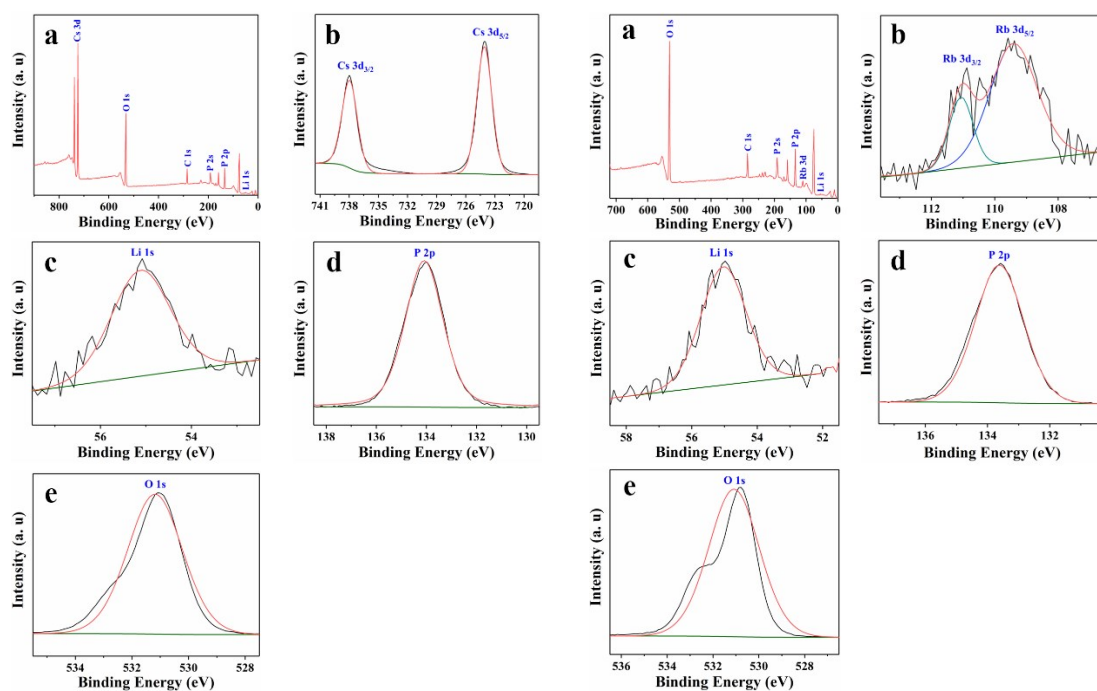


Figure S5 (a) XPS spectra of $MLiP_2O_6$. (b) M3d, (c) Li1s, (d) P2p ($2p_{3/2}$), and (e) O1s high-resolution XPS spectra.

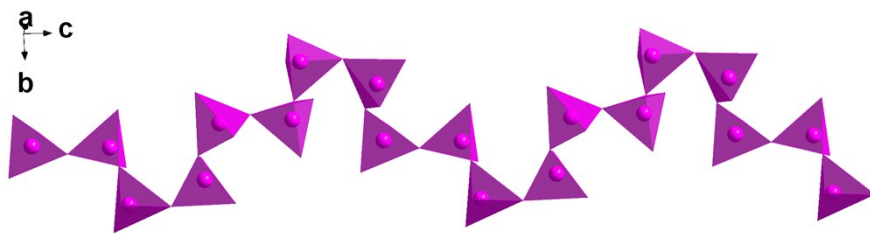
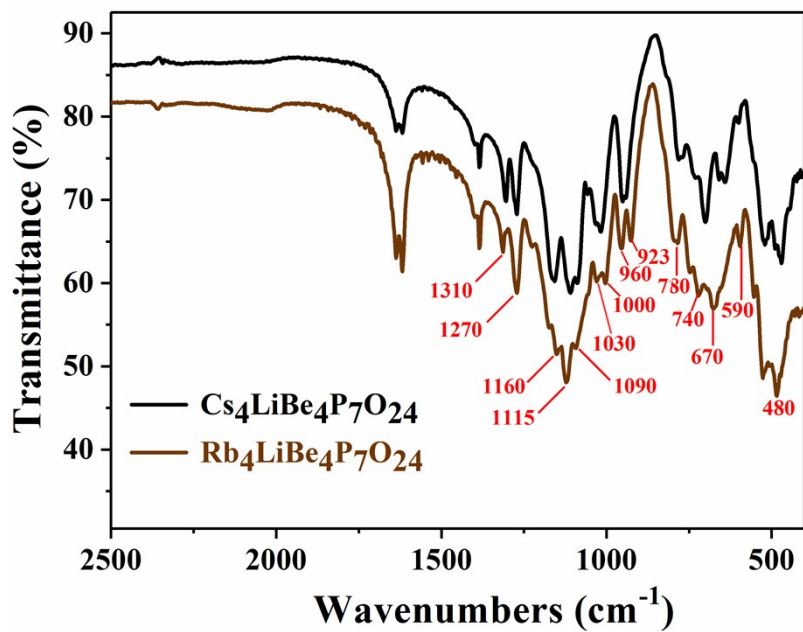
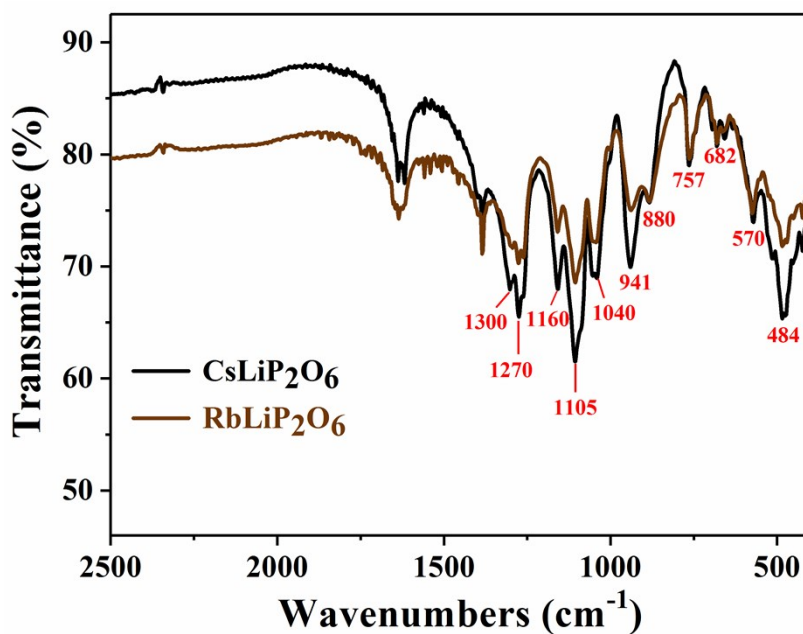


Figure S6. 1D zigzag chains of $[\text{PO}_3]_\infty$ in MLiP_2O_6 ($M = \text{Cs}, \text{Rb}$).

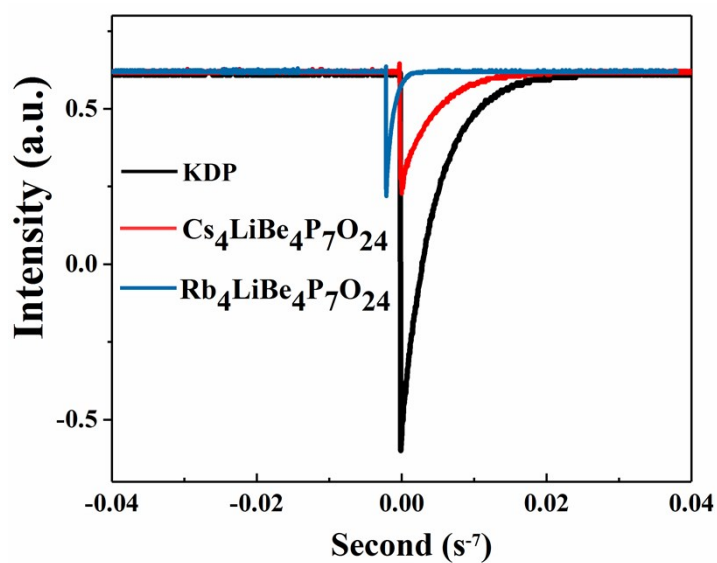


(a)

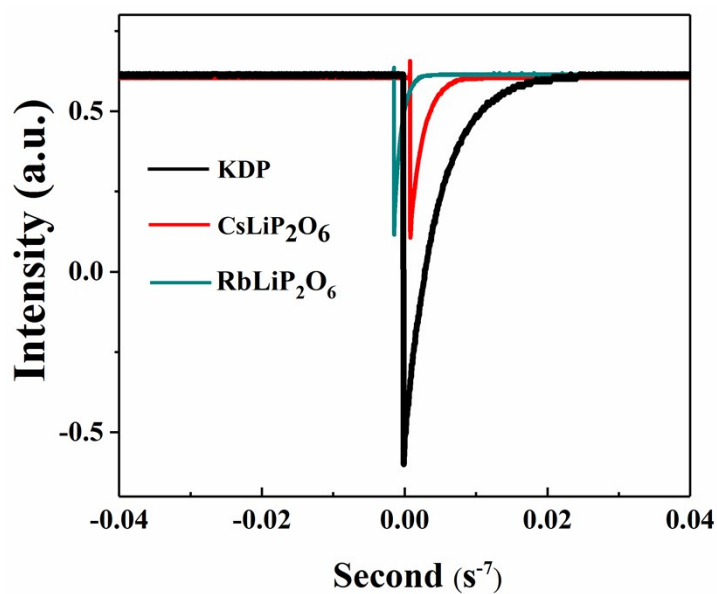


(b)

Figure S7 IR spectra (a) $\text{M}_4\text{LiBe}_4\text{P}_7\text{O}_{24}$ and (b) MLiP_2O_6 ($\text{M} = \text{Cs}, \text{Rb}$).

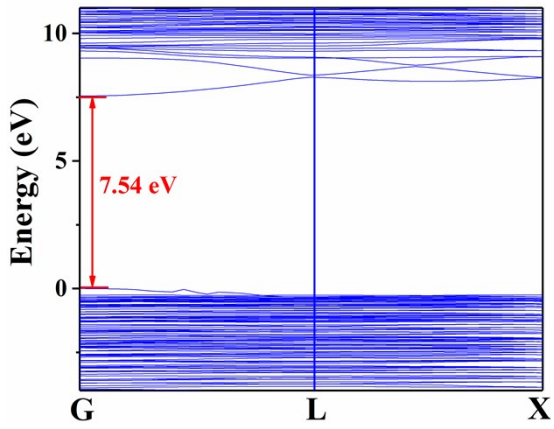
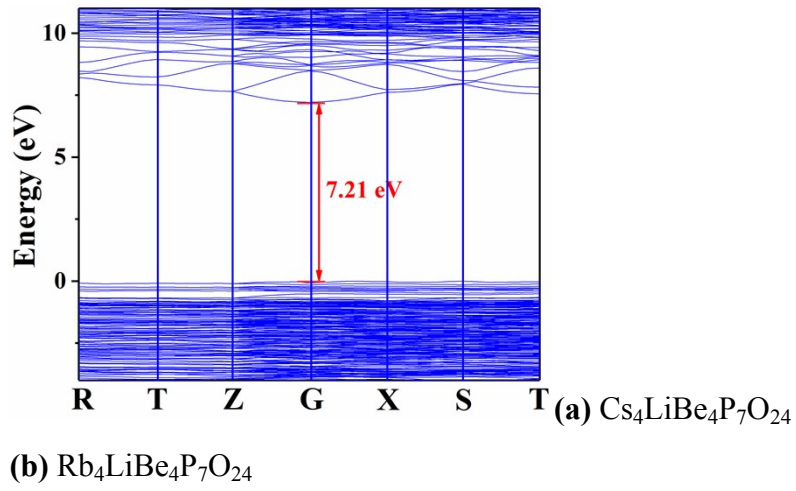
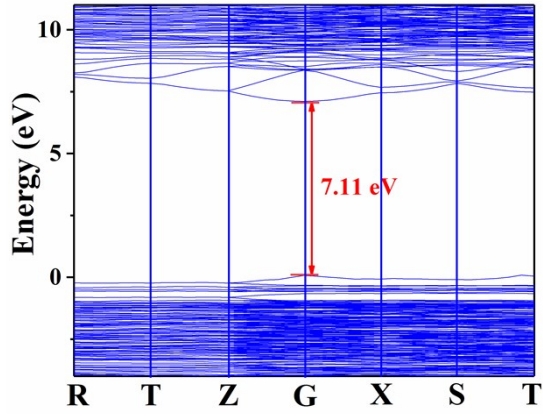


(a) $M_4LiBe_4P_7O_{24}$ (M = Cs, Rb)



(b) $MLiP_2O_6$ (M = Cs, Rb)

Figure S8. SHG signals for (a) $M_4LiBe_4P_7O_{24}$ and (b) $MLiP_2O_6$ (M = Cs, Rb) and KDP samples in the particle range 150–200 μm .



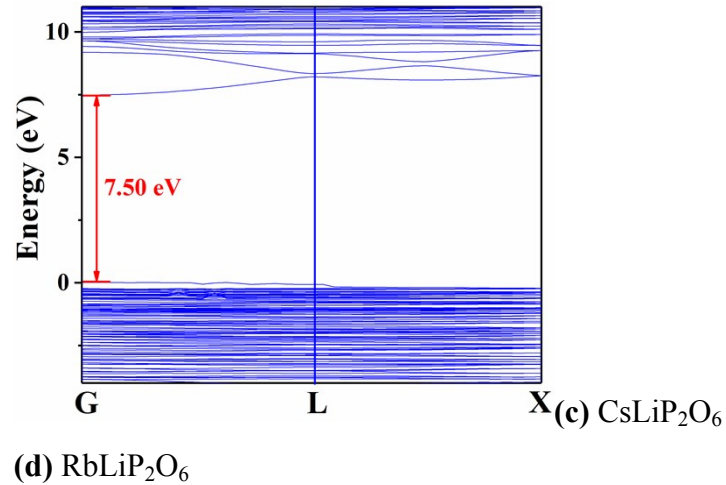


Figure S9. Electronic band structures (a) Cs₄LiBe₄P₇O₂₄, (b) Rb₄LiBe₄P₇O₂₄, (c) CsLiP₂O₆, and (d) RbLiP₂O₆.

References

1. G. M. Sheldrick, *Acta. Crystallogr. A.* 2008, **64**, 112–122.
2. A. L. Spek, *J. Appl. Crystallogr.* 2003, **36**, 7–13.
3. S. Kurtz, T. Perry, *J. Appl. Phys.*, 1968, **39**, 3798–3813.
4. G. Kresse, and J. Furthmüller, *Comput. Mater. Sci.*, 1997, **6**, 15.
5. P. E. Blochl, *Phys. Rev. B. Condens. Matter.* 1994, **50**, 17953–17979.
6. J. P. Perdew, K. Burke and M. Ernzerhof, *Phys. Rev. Lett.* 1996, **77**, 3865.
7. J. Heyd, G. E. Scuseria and M. Ernzerhof, *J. Phys. Chem. C.* 2003, **118**, 8207–8215.
8. (a) C. Aversa, J. E. Sipe, *Phys. Rev. B* 1995, **52**, 14636–14645; (b) S. N. Rashkeev, W. R. L. Lambrecht, B. Segall, *Phys. Rev. B* 1998, **57**, 3905–3919.